

Contents lists available at ScienceDirect

Fuel

journal homepage: www.elsevier.com/locate/fuel



Full Length Article

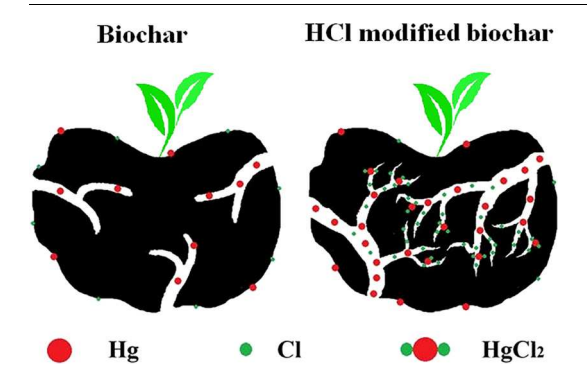
Increasing the chlorine active sites in the micropores of biochar for improved mercury adsorption



Tao Wang^a, Jiawen Wu^a, Yongsheng Zhang^{a,*}, Jun Liu^a, Zifeng Sui^a, Huicong Zhang^a, Wei-Yin Chen^b, Pauline Norris^c, Wei-Ping Pan^{a,c}

- a Key Laboratory of Condition Monitoring and Control for Power Plant Equipment, Ministry of Education, North China Electric Power University, Beijing 102206, China
- ^b Department of Chemical Engineering, University of Mississippi, 134 Anderson Hall, University, MS 38677, USA
- ^c Institute for Combustion Science and Environmental Technology, Western Kentucky University, Bowling Green, KY 42101, USA

GRAPHICAL ABSTRACT



ARTICLEINFO

Keywords: Chlorine modification Biochar Mechanism Elemental mercury Flue gas

ABSTRACT

A series of biochars were prepared from rice(RI), tobacco(TO), corn(CO), wheat(WH), millet(MI), and black bean straw(BB). These biochars were used to study the mechanism of elemental mercury(Hg 0) adsorption by hydrochloric acid modified biochars. The biochars were modified by 1 M hydrochloric acid (HCl) and then used in a fixed-bed Hg 0 adsorption experiment. As would be expected, the results indicated that HCl modification increased the Hg 0 adsorption performance of the six biochars. After modification, the Hg 0 adsorption efficiency of tobacco biochar increased from 8.2% to 100.0%, and the average Hg 0 adsorption capacity of the biochars increased by 61 times. The acid modification dissolved the metal compounds in the biochar, reducing the metal content and increasing the average surface area of the biochar. The average surface area of the raw biochars increased from 29.9 to $110.1 \, \text{m}^2/\text{g}$ after HCl modification. The extra surface area was mostly created in the micropores, leading to a significant increase in the amount of micropores. These micropores effectively adsorbed the Cl atoms, which acted as active sites for Hg 0 . In the adsorption process, Hg 0 diffused into the interior of modified biochars via mesopores, and finally the adsorbed Cl in the micropores reacted with Hg 0 to form HgCl $_2$.

1. Introduction

Mercury has received growing worldwide concern due to its

toxicity. Mercury emission from coal combustion is one of the largest sources of mercury pollution. Coal consumption in China accounted for 50.6% of global mercury coal consumption in 2016. It is estimated that

E-mail address: yszhang@ncepu.edu.cn (Y. Zhang).

^{*} Corresponding author.

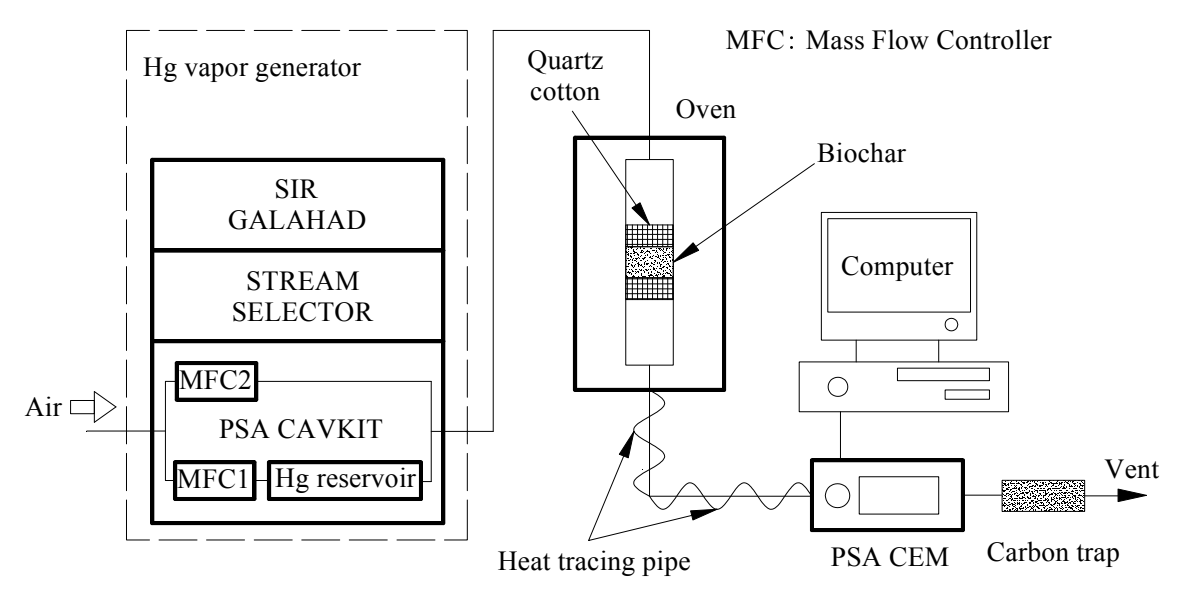


Fig. 1. Schematic diagram of Hg⁰ adsorption.

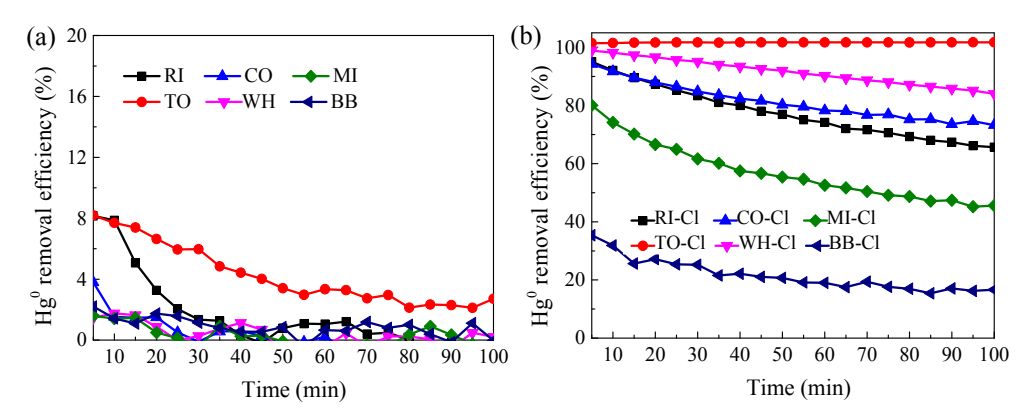


Fig. 2. Hg⁰ removal efficiency of raw and modified biochars.

70% of the mercury pollution in China comes from coal combustion, which accounts for 25%–40% of global mercury emissions [1–4]. ${\rm Hg^0}$ is more difficult to remove than oxidized or particle-bound mercury due to its low reactivity, low water solubility and high volatility. Activated carbon injection methods have been reported as the most promising technology for ${\rm Hg^0}$ removal [5–7]. Activated carbon, injected into the flue gas before the particulate control devices, adsorbs the ${\rm Hg^0}$ from the flue gas and is then captured by the particulate control devices. However, the high operational cost of activated carbon injection limits large-scale applications. Discussions regarding the development of low-cost adsorbents have dominated research in recent years.

Biochar pyrolyzed from agricultural biomass would be attractive as a low cost and abundant sorbent. Unfortunately, the Hg⁰ adsorption capacity of unactivated biochars is at least 2–3 orders of magnitude lower than activated carbon [8]. Therefore, many physical and chemical activation techniques have been used to promote biochar adsorption capacity. Li et al. reported that the adsorption capacity of chemically modified biochar was 2–3 greater than biochar modified by physical techniques [9]. Chemical techniques mainly add active functional groups on the biochar by acid [10–13], alkali [14,15], metal [16–18], sulfur [19–23] and halogen [24–29] modification, which promotes the removal of elementary mercury. Hg⁰ can react with Fe³⁺ to form oxidized mercury, resulting in an increase in Hg⁰ removal efficiency from 40.0% to 99.9% after FeCl₃ modification [30]. Hg⁰ removal efficiency increased by 32.1% after KOH modification [14] and Hg⁰ adsorption capacity of NaOH modified coconut husk biochar

increased by 31.0% [31]. In a study by Klasson et al., HCl modified biochar adsorbed over 95% of the ${\rm Hg^0}$ from the flue gas [32]. In another study by Johari et al., the Hg⁰ adsorption capacity of HCl modified biochar reached 6067 µg/g and the Hg⁰ removal efficiency of HCl-impregnated biochar was 34 times greater than that of raw biochar [11]. Though previous studies have shown that HCl modification leads to an obvious increase in the Hg⁰ adsorption capacity, mechanisms of Hg⁰ adsorption on HCl modified biochar are not clear. Johari [11] reported that HCl modification enlarged the surface area, improving the physical adsorption of Hg⁰. Klasson's work showed no direct correlation between Hg⁰ adsorption capacity and surface area after HCl modification and indicated that Hg⁰ was adsorbed via chemisorption [32]. While Shen indicated that HCl modification added the C-Cl group on the surface of biochar, which reacted with Hg⁰ to form HgCl₂ [33].Clearly, more research is needed to determine the mechanism of Hg⁰ adsorption on HCl modified biochar.

In this paper, rice, tobacco, corn, wheat, millet, and black bean straw were prepared in high purity nitrogen at 600 °C to produce biochars, which were then impregnated by 1 M HCl. The effect of HCl modification on Hg⁰ adsorption by six biochars was studied. Biochar composition, Brunauer–Emmett–Teller (BET), Fourier transform infrared spectroscopy (FTIR), X-ray photoelectron spectroscopy (XPS), thermogravimetric analysis (TGA), inductively coupled plasma optical emission spectrometry (ICP-OES), temperature programmed desorption (TPD), and Ion chromatography were used to discuss the possible mechanisms of Hg⁰ adsorption on HCl modified biochar.



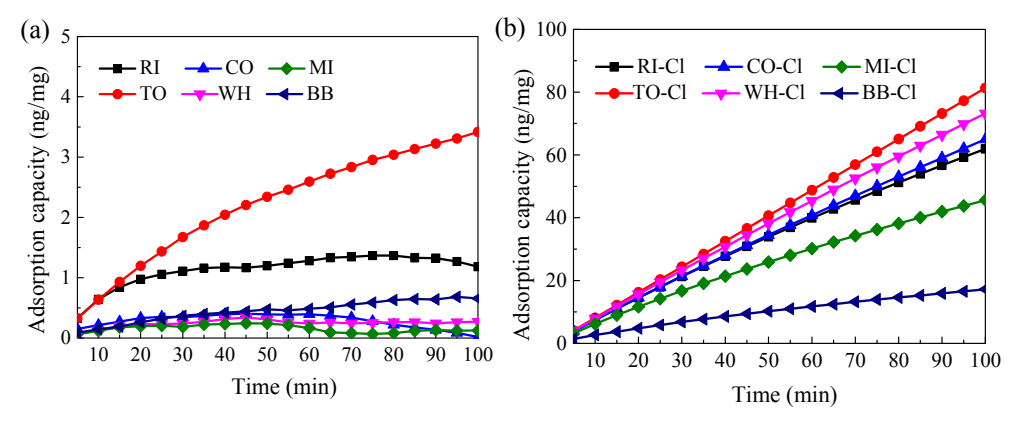


Fig. 3. Hg⁰ adsorption capacity of raw and modified biochars.

Table 1 Properties of biochars.

Sample	Ultima	ate ana	lysis (wt	:%)		Proximate analysis (wt%)			
	С	Н	O ^a	N	S	Moisture	Volatile matter	Fixed carbon	Ash
RI	47.8	0.6	10.3	0.6	0.5	4.7	9.3	45.8	40.2
TO	42.3	0.9	15.0	1.5	0.5	5.7	15.8	38.7	39.8
CO	47.9	1.0	25.7	2.2	0.7	5.9	12.9	58.7	22.5
WH	65.3	0.9	10.0	0.5	0.7	6.0	12.4	59.0	22.6
MI	56.8	1.2	7.6	0.9	0.6	5.0	12.8	49.3	32.9
BB	59.5	0.9	8.4	2.1	0.6	4.6	18.5	48.4	28.5
RI-Cl	54.8	0.9	9.4	0.8	0.6	5.2	8.9	52.4	33.5
TO-Cl	68.3	1.3	19.8	2.6	0.7	9.8	12.7	70.2	7.3
CO-Cl	70.3	0.9	11.2	2.6	0.8	6.5	11.5	67.8	14.2
WH-Cl	73.4	0.6	10.8	0.2	0.8	5.7	11.1	69.0	14.2
MI-Cl	62.8	0.8	12.0	0.6	0.7	5.4	11.0	60.5	23.1
BB-Cl	70.8	1.1	9.7	2.1	0.8	6.2	14.4	63.9	15.5

 $^{^{}a}$ O = 100 - (C + N + H + S + Ash).

Table 2
Metal content of raw and modified biochars.

Sample	Metal content (mg/g)							
	Al	Ca	Cu	Fe	Mg			
RI	1.0	24.2	0.5	1.5	3.5			
TO	0.6	143.0	1.8	0.4	19.4			
CO	3.0	23.8	0.5	3.9	10.0			
WH	4.5	29.7	0.3	6.0	4.7			
MI	3.5	37.2	0.3	4.1	11.6			
BB	2.5	78.5	0.2	2.5	17.8			
RI-Cl	0.2	2.3	0.1	0.2	0.6			
TO-Cl	0.2	8.8	0.4	0.1	3.0			
CO-Cl	1.6	1.9	0.2	1.1	5.0			
WH-Cl	2.1	2.8	0.2	1.6	1.7			
MI-Cl	1.9	3.0	0.1	1.1	4.3			
BB-Cl	1.3	5.4	0.1	0.5	7.8			

2. Materials and methods

2.1. Preparation of biochar

Rice, tobacco, corn, wheat, millet, and black bean straw were washed by deionized water to remove unwanted impurities as a pretreatment. The washed samples were dried at $110\,^{\circ}\text{C}$ in an oven for $24\,\text{h}$ and then crushed to 100--200 mesh. The details of the preparation process were described in our previous work [34]. Briefly, ten grams of biomass samples were wrapped in a 200-mesh copper mesh and placed in a $500\,\text{mm}$ long reactor. The reactor was swept by high purity N_2 at $300\,\text{mL/min}$, which was purified by copper mesh at $500\,^{\circ}\text{C}$ to remove

trace oxygen prior to the pyrolysis process [35]. The reactor was heated to 600 °C at 10 °C/min in a vertical tube furnace and held at 600 °C for 60 min, then cooled to room temperature in $\rm N_2$. The biochar was prepared from rice, tobacco, corn, wheat, millet, and black bean straw, denoted as RI, TO, CO, WH, MI and BB, respectively. Approximately 500 mg of biochar was impregnated in 50 mL HCl for 12 h, then washed by deionized water. The samples were dried at 110 °C in an oven for 24 h. The modified biochars were denoted as RI-Cl, TO-Cl, CO-Cl,WH-Cl, MI-Cl and BB-Cl, respectively.

2.2. Mercury adsorption experiment

The experimental apparatus schematic for mercury adsorption is shown in Fig. 1 [34]. Mercury adsorption performance was studied in a fixed-bed system. Compressed air was used to transport Hg 0 from the mercury source (PSA 10.536 Cavkit). Total gas was set at $2\,L/min$ and the initial Hg 0 concentration was controlled at $20\,\mu g/m^3$. A 0.05 g sample was placed in the center of the reactor with an inner diameter of 6 mm and a length of 250 mm. The reactor was placed in an oven and the temperature was set at 150 °C. Heat tracing pipe maintained at 140 °C prevented Hg 0 condensation. The Hg 0 concentration was monitored by a PSA Continuous Emission Monitor (CEM). The biochar Hg 0 removal efficiency (η) was calculated by Eq. (1):

$$\eta \text{ (\%)} = \frac{C_{\text{in}} - C_{\text{out}}}{C_{\text{in}}} \times 100 \tag{1}$$

where $C_{\rm in}$ and $C_{\rm out}$ are the instantaneous Hg^0 concentration of the inlet and outlet, respectively.

To evaluate the Hg⁰ adsorption capacity per unit quality of biochar, the following definition was used:

$$q_t = \frac{Q}{m} \int_0^t (C_{in} - C_{out}) dt \approx \frac{QC_{in}\Delta t}{m} \sum_{i=0}^n \left(1 - \frac{C_{out}^i + C_{out}^{i+1}}{2C_{in}} \right) \tag{2}$$

where q_t is the Hg^0 adsorption capacity per unit quality of biochar, Q is the flow rate of flue gas, m represents the mass of the sorbent, C_{in} is the initial inlet Hg^0 concentration, C_{out} represents the outlet Hg^0 concentration at time t, Δt is the sampling time interval and Δt was 5 min in this work, C_{out}^i and C_{out}^{i+1} are the outlet Hg^0 concentration at time i and i+1, respectively.

2.3. Characterization

Ultimate analysis values were measured by an elemental analyzer (EA3000). Proximate analysis was analyzed using a TGA701. Thermal stability was evaluated using a thermogravimetric analyzer (TAQ600). The BET surface area, pore width, and pore volume were measured using a JW-BK200C. Fourier transform infrared (FTIR) spectroscopy (PerkinElmer) was used to identify the surface functional groups. The

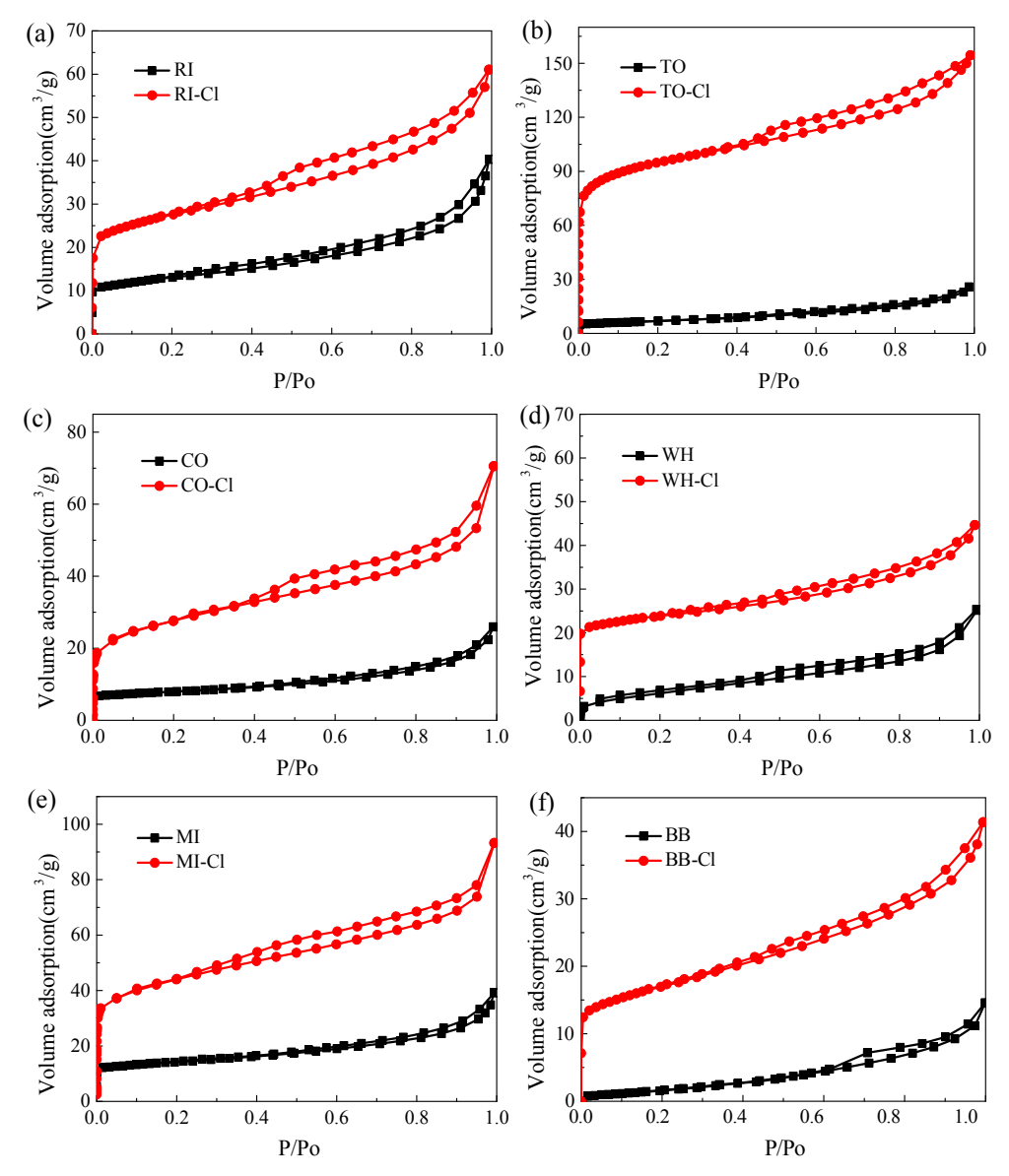


Fig. 4. N₂ adsorption-desorption isotherms of raw and modified biochars.

 Table 3

 Textural characteristics of raw and modified biochars.

-	Textural characteristics of faw and modified blochars.									
-	Sample	BET surface area(m ² / g)	Average pore width (nm)	Micropore volume ^a (cm ³ /g)	Mesopore volume ^b (cm ³ /g)	Total pore volume (cm ³ /g)				
	RI	46.9	5.3	0.009	0.054	0.063				
	TO	23.9	6.7	0.002	0.039	0.041				
	CO	29.0	5.6	0.006	0.035	0.041				
	WH	23.4	5.7	0.005	0.066	0.071				
	MI	51.9	4.7	0.012	0.049	0.061				
	BB	4.5	19.8	0.002	0.024	0.026				
	RI-Cl	99.7	3.8	0.022	0.073	0.095				
	TO-Cl	353.4	2.7	0.106	0.139	0.245				
	CO-Cl	93.3	2.2	0.026	0.137	0.163				
	WH-Cl	88.6	3.1	0.026	0.044	0.070				
	MI-Cl	144.7	2.4	0.035	0.123	0.158				
	BB-Cl	60.7	4.2	0.010	0.054	0.064				

^a Pore width = 0-2 nm,

elemental states of C, Cl and Hg on the biochar surface were analyzed using a XPS instrument (PHI quantera SXM). The metal concentrations were measured by ICP-OES (Leeman Labs, Prodigy). A temperature programmed desorption (TPD) technique was used to determine the modes of mercury compounds. The TPD technique consisted of a 0.2 g sample of biochar with adsorbed ${\rm Hg}^0$ packed in a quartz tube equipped with an electrical furnace that heated the tube from 30 °C to 800 °C at 8.5 °C/min in ${\rm N}_2$. The concentration of released mercury was monitored by a mercury analyzer (Lumex RA-915+). The chlorine content was evaluated using a Dionex ICS-1100 IC instrument [36].

3. Results and discussion

3.1. Hg⁰ adsorption using biochar

The Hg^0 removal efficiency and Hg^0 adsorption capacity of raw biochars in Figs. 2(a) and 3(a) were studied by our previous work [34], while that of HCl modified biochars were shown in Figs. 2(b) and 3(b). The six raw biochars exhibited similar adsorption performance; the initial removal efficiencies were less than 9.0% and decreased gradually in 100 min. The TO showed the best activity for Hg^0 adsorption; the

^b Pore width = 2-300 nm.

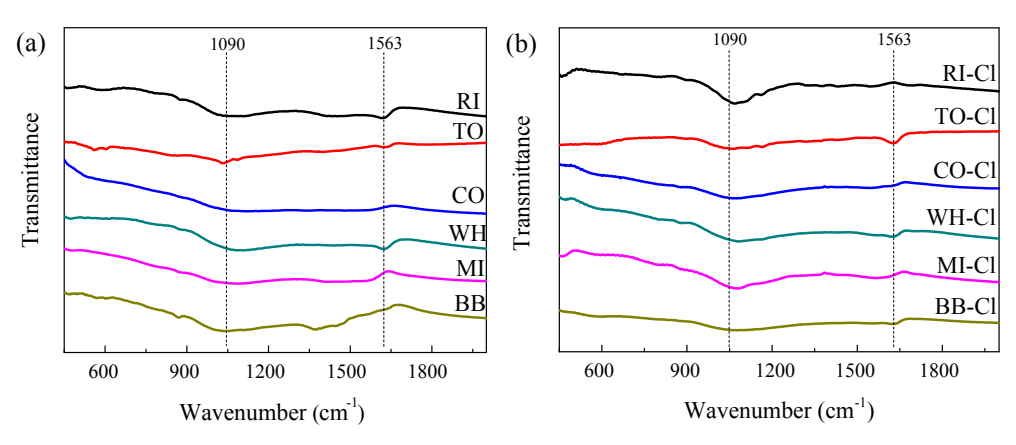


Fig. 5. The FTIR spectra for raw and modified biochars.

initial Hg⁰ removal efficiency was 8.2% and the adsorption capacity was 3.4 ng/mg in 100 min. Li [37] also reported that the Hg⁰ removal efficiency of raw biochar was 1.2%, and then decreased to 0 after 50 min. Figs. 2(d) and 3(d) show the results of Hg⁰ removal performance by the HCl modified biochars. HCl activation obviously promoted Hg⁰ adsorption; the initial Hg⁰ removal efficiencies of RI-Cl, TO-Cl, CO-Cl, WH-Cl, MI-Cl and BB-Cl were 95.0%, 100.0%, 94.3%, 98.9%, 80.0% and 35.4%, respectively. Moreover, the Hg⁰ removal efficiencies of the modified biochars remained relatively stable for 100 min. Modified tobacco biochar had the best Hg⁰ adsorption performance, 100.0% Hg⁰ removal efficiency after 100 min. The adsorption capacities of RI-Cl, TO-Cl, CO-Cl, WH-Cl, MI-Cl and BB-Cl were 61.9, 81.3, 65.0, 73.2, 43.8 and 17.2 ng/mg, respectively. The adsorption capacity of modified tobacco biochar was 24 times higher than that of raw tobacco biochar.

3.2. Biochar composition

The ultimate and proximate analysis were shown in Table 1, and that of raw biochars were studied by our previous work [34]. The carbon (C) concentration was between 42.3% and 65.3%, and was the main element in the raw biochars, followed by oxygen (O) between 7.6% and 25.7%. Hydrogen (H), nitrogen (N) and sulfur (S) concentrations were less than 3.0%. After HCl modification, the carbon concentration of all six biochars increased, with the largest increase in the tobacco biochar from 42.3% to 68.3%. The fixed carbon percentage increased after HCl modification, with the largest increase in the tobacco biochar. This result is consistent with the carbon concentration in the ultimate analysis. The volatile matter content decreased slightly after modification for the six biochars. The decrease in volatile matter leads to an increase in the pore volume of the biochars [11], and also contributes to the thermal stability of biochars (see Supplementary material). Ash was another main component in the raw biochars, RI and TO had relatively high ash percentages with 40.2% and 39.8%, respectively. After modification, the ash content of all samples decreased dramatically. The ash content in RI-Cl, TO-Cl, CO-Cl, WH-Cl, MI-Cl and BB-Cl decreased by 6.7%, 32.5%, 8.3%, 8.4%, 9.8% and 13.0%, respectively. Metals, such as aluminum (Al), calcium (Ca), copper (Cu), iron (Fe) and magnesium (Mg), in the ash provide active sites to oxidize the elemental mercury to oxidized mercury [38-40]. As shown in Table 2, the concentrations of Al, Ca, Cu, Fe and Mg in biochars were analyzed before and after modification. The main metal in the ash of the six raw samples was Ca, followed by Mg. The concentrations of Al, Cu and Fe were between 0.2% and 6.0%. After modification, the concentrations of Al, Ca, Cu, Fe and Mg decreased in all samples, which greatly reduced the amount of ash. TO had the highest Ca content, 143.0 mg/g, which decreased rapidly to 8.8 mg/g after modification. Therefore, the enhancement of Hg⁰ adsorption by HCl modified biochars was not related to metals.

3.3. Textural characteristics

The N₂ adsorption-desorption isotherms for the biochars are shown in Fig. 4. All biochars exhibited a type II isotherm and a type H4 hysteresis loop, indicating that all biochars had a mostly mesoporous structure [41,42]. As shown in Table 3, mesopore volume accounted for most of the total pore volume. The raw biochars possessed relatively low BET surface area, and a small micropore volume, ranging from 0.002 to 0.012 m³/g. After HCl modification, both micropore volume and mesopore volume increased, especially the increase in micropore volume. An obvious increase in N2 adsorption occurs at low relative pressure after modification in Fig. 4, indicating that HCl modification created a large amount of micropores. The mesopores act as the entry portal and transportation channel, while the micropores serve as active sites for adsorption [16]. The slit-shaped micropores in biochars provide a stronger adsorption capacity than the external surface [6]. The micropores play a pivotal part in the adsorption of Hg (< 2nm) and Cl (< 2nm), depending on the complexation [8]. TO has the largest growth in surface area and pore volume. Micropore volume of raw tobacco biochar, increased from 0.002 m³/g to 0.106 m³/g. HCl modification reduced the ash in biochars. The extra surface area was mostly created in the micropore region [32]. This is confirmed by the largest decrease in ash content of tobacco biochar after modification.

3.4. FTIR analysis

Our previous research [34] studied the surface functional groups of raw biochars as shown in Fig. 5(a), while that of modified biochars were presented in Fig. 5(b). The wide adsorption peak at around 1090 cm⁻¹ represents the C–O stretching. The peak at 1563 cm⁻¹ is attributed to C=O stretching vibrations of various oxygen functional groups, such as carboxyl, ester and anhydride. The intensity of the peak at 1090 cm⁻¹ did increase after HCl modification, but there were no new peaks. Bohli [10] generally confirms that acid modification increases the carboxylic and phenol groups on the sample surface. However, the peak at 1090 cm⁻¹ also represents Cl–C–Cl stretching, which can overlap with the C–O absorption peak. More information on C and Cl on the surface of biochar was determined by XPS analysis.

3.5. XPS analysis

Biochars were analyzed by XPS to identify chemical states on the surface of raw and modified biochars. The XPS spectra of RI, TO, RI-Cl and TO-Cl are shown in Fig. 6. The C and Cl concentrations and relative intensity of C and Cl functional groups were summarized in Table 4. As shown in Fig. 6(a) and (b), the low peak located at 283.1–284.1 eV contributed to C-C, the peak in the range of 284.4–285.2 eV contributed to C-O, the binding energy peak at 286.2–287.0 eV

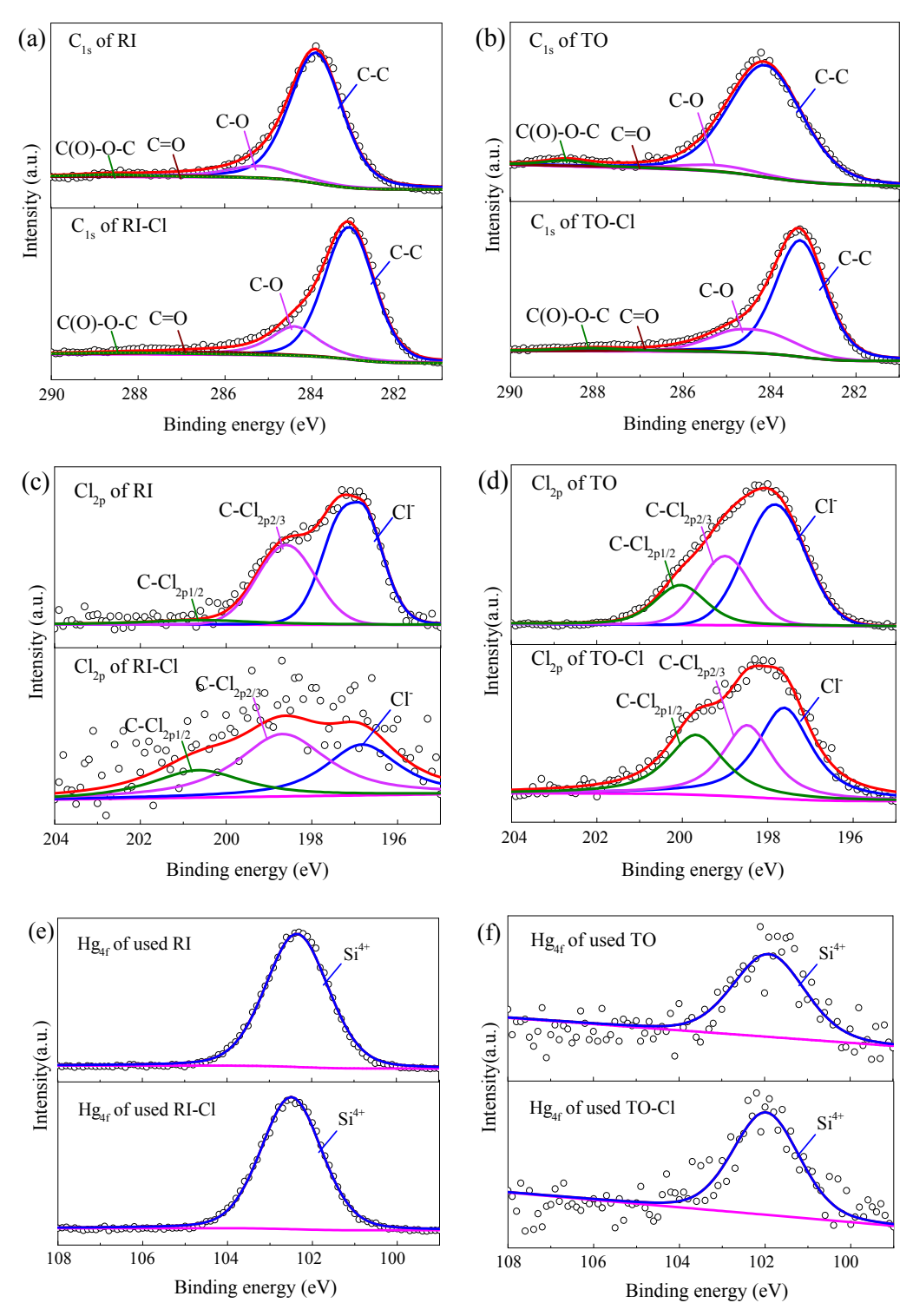


Fig. 6. XPS spectra of C_{1s} , Cl_{2p} and Hg_{4f} for biochars.

Table 4Related functional groups obtained from XPS spectra.

Sample	Atom conten	Atom content (%)		Relative intensity (%)						
	С	Cl	C-C	C-O	C=O	C(O)-O-C	Cl-	C-Cl _{2p2/3}	C-Cl _{2p1/2}	
RI	71.8	1.5	83.7	11.4	2.0	2.9	60.8	34.2	5.0	
RI-Cl	72.1	0.3	74.3	19.6	3.8	2.3	31.4	47.3	21.3	
TO	60.8	7.8	88.7	6.0	1.5	3.8	54.5	27.5	18.0	
TO-Cl	86.9	1.0	73.1	21.8	1.9	3.2	41.6	30.0	28.4	

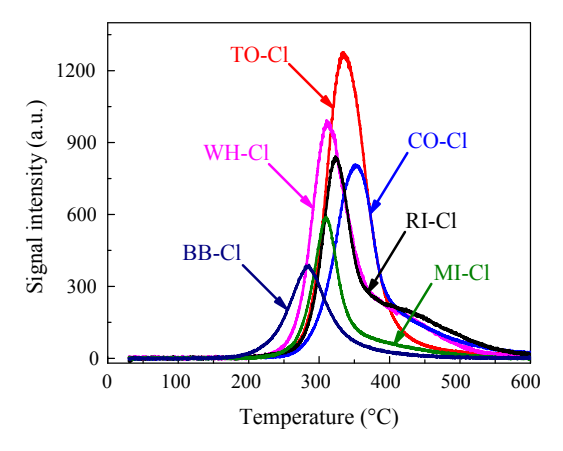


Fig. 7. Temperature programmed desorption of modified biochars.

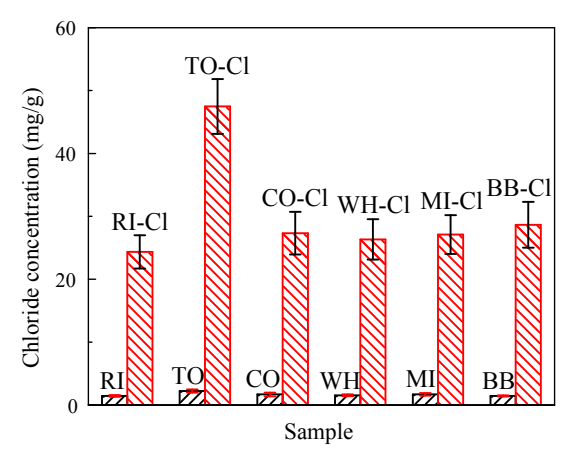


Fig. 8. Chlorine concentrations of raw and modified biochars.

contributed to C=O, and the peak located at 288.1–288.7 eV contributed to C(O)–O–C. The carbon concentration on the surface of the modified rice and tobacco biochar was larger than the corresponding raw biochars. This is consistent with the ultimate analysis data in Table 1. HCl modification slightly decreased the relative intensity of C(O)–O–C, but increased the relative intensity of C–O and C=O on the biochar surface. Previous research [43,44]indicates that C–O and C=O groups play a key role in Hg⁰ adsorption. Among the oxygen functional groups, the C–O groups had the largest increase. After chemical activation, the rice biochar C–O groups increased from 11.4% to 19.6% and the tobacco biochar increased from 6.0% to 21.8%.These results are consistent with the increase in C–O stretching at 1090 cm⁻¹ in the FTIR spectra.

It is widely accepted that chlorine groups promote Hg⁰ adsorption. The effect of HCl modification on Cl_{2p} is shown in Fig. 6(c) and (d). The low peak at 196.8-197.8 eV corresponds to ionic chlorine (Cl-), and the other two peaks at 198.5-199.0 eV and 200.0-200.7 eV correspond to C-Cl_{2p2/3} and C-Cl_{2p1/2}, respectively. The relative Cl intensities for RI and TO are 60.8% and 54.5%, representing the predominant phase of rice and tobacco biochar. The relative Cl⁻ intensities for RI-Cl and TO-Cl decreased to 31.4% and 41.6%, respectively. In contrast, the total C-Cl groups of RI and TO increased from 39.2% and 45.5% to 68.6% and 58.4% after modification, respectively. Shen [33] also found that HCl modification improved the relative intensity of C-Cl groups. These groups act as chemisorption sites and oxidize Hg^0 into Hg^{2+} . However, the Cl content of RI and TO significantly decreased from 1.5% and 7.8% to 0.3% and 1.0% after modification, respectively. Therefore, the real content of C-Cl groups decreased after HCl modification, if the significant decrease in the Cl content on the surface of biochars is considered. The Hg4f spectrum after adsorption experiment was presented in Fig. 6(e) and (f), the peak at 102.0–102.4 eV corresponds to Si^{4+} .The $\mathrm{Hg_{4f}}$ peak at around 104.3 eV [45], did not appear on XPS spectra, indicating that the adsorption of $\mathrm{Hg^0}$ by C–Cl groups on the surface of biochars can even be ignored.

3.6. Temperature programmed desorption of Hg⁰

Hg-TPD was used to identify the modes of mercury compounds in modified biochars after adsorption. As shown in Fig. 7, the mercury desorption peaks for the samples ranged from 283 to 351 °C, but were mainly concentrated at 310 °C. This desorption temperature should correspond to mercury chloride (HgCl₂) [46]. Wu reported that the desorption peak of HgCl₂ on activated carbon were 290 °C [46] and 350 °C [47], respectively. The interaction between Hg and chemisorption site, makes HgCl2 more stable on the surface of activated carbon. CO-Cl had the highest desorption peak temperature at 351 °C, while BB-Cl had the lowest, indicating that the interaction between BB-Cl and HgCl₂ was weaker than the other five samples. XPS spectra indicated that chlorine on the surface of rice and tobacco biochars decreased by 80.0% and 87.2% after HCl modification. However, the adsorbed mercury compounds were present as HgCl2 on modified biochars. It is believed that more chlorine was adsorbed on the internal surface of the modified biochars and oxidized Hg^0 to Hg^{2+} . As shown in Fig. 8, chlorine concentration was less than 2 mg/g for the six raw biochars, while the concentration for RI-Cl, TO-Cl, CO-Cl, WH-Cl, MI-Cl and BB-Cl was 24.4, 47.5, 27.3, 26.3, 27.1 and 28.7 mg/g, respectively. The Cl atoms mainly attached on the internal surface of modified biochars. TO-Cl had the largest chlorine concentration at 47.5 mg/g, in accordance with its Hg⁰ adsorption capacity. The chlorine concentration of BB-Cl slightly exceeded that of RI-Cl, CO-Cl, WH-Cl and MI-Cl, mainly because the interaction between modified black bean biochar and Cl was weak. This resulted in the Cl more easily desorbing from the BB-Cl, as evidenced by the low desorption temperature, 283 °C, observed in the Hg-TPD data shown in Fig. 7.

Hydrochloric acid washes away metals from biochars, thereby simultaneously decreasing the ash content and increasing the number of micropores and mesopores. The extra surface area was mostly created in the micropore region. The mesopores act as an entrance and transportation channel, while the micropores serve as active sites for adsorption of Cl, depending on the complexation. In the adsorption process, Hg⁰ transferred from the gas phase to the internal surface of modified biochars through mesopores, was then captured by the adsorbed Cl in the micropores via a chemical adsorption process, and finally oxidized to Hg²⁺.

4. Conclusion

Biochars pyrolysed from rice, tobacco, corn, wheat, millet, and black bean straw were used to study the mechanism of elemental mercury removal by hydrochloric acid modified biochars. The six raw biochars exhibited similar adsorption performance and the initial removal efficiencies were less than 9.0%. After 1 M hydrochloric acid modification, the Hg⁰ adsorption efficiency of tobacco biochar increased from 8.2% to 100.0%, and the average Hg⁰ adsorption capacity of the biochars increased by 61 times. Biochar composition, BET, FTIR, XPS, TGA, ICP-OES, Hg-TPD, and Ion chromatography were used to discuss the possible mechanisms of Hg⁰ adsorption on HCl modified biochar. Hg-TPD indicated that the modes of mercury compounds were HgCl₂ in modified biochars after adsorption. Chlorine concentration for six biocahrs increased from about 2 mg/g to above 24 mg/g after modification. However, The Cl on the surface of RI and TO significantly decreased from 1.5% and 7.8% to 0.3% and 1.0% after modification, respectively. Therefore, the Cl atoms mainly attached on the internal surface of modified biochars. Hydrochloric acid washes away metals from biochars, thereby simultaneously increasing the number of micropore and mesopore, especially the increase in micropore, which

effectively adsorbed the Cl atoms. In the adsorption process, Hg⁰ diffused into the internal surface of modified biochars through mesopores, was then reacted with the adsorbed Cl in the micropores to form HgCl₂.

Acknowledgements

This work was supported by National Natural Science Foundation of China (51706069), Fundamental Research Funds for the Central Universities (2017JQ002) and the US National Science Foundation (1632899).

Appendix A. Supplementary data

Supplementary data associated with this article can be found, in the online version, at http://dx.doi.org/10.1016/j.fuel.2018.05.028.

References

- Wang S, Zhang L, Wang L, Wu Q, Wang F, Hao J. A review of atmospheric mercury emissions, pollution and control in China. Front Environ Sci Eng 2014;8:631–49.
- [2] Liu Y, Wang Q. Removal of elemental mercury from flue gas by thermally activated ammonium persulfate in abubble column reactor. Environ Sci Technol 2014;48:12181–9.
- [3] Wang J, Liang Y, Jin Q, Hou J, Liu B, Li X, et al. Simultaneous removal of graphene oxide and chromium(VI) on the rare earth doped titanium dioxide coated carbon sphere composites. ACS Sustainable Chem Eng 2017;6:5550–61.
- [4] Xu C, Xin T, Xu G, Li X, Liu W, Yang Y. Thermodynamic analysis of a novel solarhybrid system for low-rank coal upgrading and power generation. Energy 2017;141:1737–49.
- [5] Shu T, Lu P, He N. Mercury adsorption of modified mulberry twig chars in a simulated flue gas. Bioresour Technol 2013;136:182–7.
- [6] His HC, Tsai CY, Kuo TH, Chiang CS. Development of low-concentration mercury adsorbents from biohydrogen-generation agricultural residues using sulfur impregnation. Bioresour Technol 2011;102:7470–7.
- [7] Xu Y, Zeng X, Luo G, Zhang B, Xu P, Xu M, et al. Chlorine-Char composite synthesized by co-pyrolysis of biomass wastes and polyvinyl chloride for elemental mercury removal. Fuel 2016;183:73–9.
- [8] Gomez-Eyles JL, Yupanqui C, Beckingham B, Riedel G, Gilmour C, Ghosh U. Evaluation of biochars and activated carbons for in situ remediation of sediments impacted with organics, mercury, and methylmercury. Environ Sci Technol 2013;47:13721–9.
- [9] Li G, Wang S, Wang F, Wu Q, Tang Y, Shen B. Role of inherent active constituents on mercury adsorption capacity of chars from four solid wastes. Chem Eng J 2017:307:544–52.
- [10] Bohli T, Ouederni A. Improvement of oxygen-containing functional groups on olive stones activated carbon by ozone and nitric acid for heavy metals removal from aqueous phase. Environ Sci Pollut Res Int 2016;23:1–10.
- [11] Johari K, Saman N, Song ST, Cheu SC, Kong H, Mat H. Development of coconut pith chars towards high elemental mercury adsorption performance – effect of pyrolysis temperatures. Chemosphere 2016;156:56–68.
- [12] Tan Z, Qiu J, Zeng H, Liu H, Xiang J. Removal of elemental mercury by bamboo charcoal impregnated with $\rm H_2O_2$. Fuel 2011;90:1471–5.
- [13] Xu H, Shen B, Yuan P, Lu F, Tian L, Zhang X. The adsorption mechanism of elemental mercury by HNO₃-modified bamboo char. Fuel Process Technol 2016:154:139–46.
- [14] Tan G, Sun W, Xu Y, Wang H, Xu N. Sorption of mercury (II) and atrazine by biochar, modified biochars and biochar based activated carbon in aqueous solution. Bioresour Technol 2016;211:727–35.
- [15] Biniak S, Pakuła M, Szymański GS, Świątkowski A. Effect of activated carbon surface oxygen- and/or nitrogen-containing groups on adsorption of copper(II) Ions from aqueous solution. Langmuir 1999;15:6117–22.
- [16] Tan Z, Sun L, Xiang J, Zeng H, Liu Z, Hu S, et al. Gas-phase elemental mercury removal by novel carbon-based sorbents. Carbon 2012;50:362–71.
- [17] Yang W, Liu Y, Wang Q, Pan J. Removal of elemental mercury from flue gas using wheat straw chars modified by Mn-Ce mixed oxides with ultrasonic-assisted impregnation. Chem Eng J 2017;326:169–81.
- [18] Zhao B, Xu XY, Xu SC, Chen X, Li HB, Zeng FQ. Surface characteristics and potential ecological risk evaluation of heavy metals in the bio-char produced by co-pyrolysis from municipal sewage sludge and hazelnut shell with zinc chloride. Bioresour Technol 2017;243:375–83.
- [19] Ie IR, Hung CH, Jen YS, Yuan CS, Chen WH. Adsorption of vapor-phase elemental mercury (Hg⁰) and mercury chloride (HgCl₂) with innovative composite activated carbons impregnated with Na₂S and S⁰ in different sequences. Chem Eng J 2013:229:469–76.
- [20] Saha A, Abram DN, Kuhl KP, Paradis J, Crawford JL, Sasmaz E, et al. An X-ray

- photoelectron spectroscopy study of surface changes on brominated and sulfurtreated activated carbon sorbents during mercury capture: performance of pellet versus fiber sorbents. Environ Sci Technol 2013;47:13695–701.
- [21] Li G, Shen B, Lu F. The mechanism of sulfur component in pyrolyzed char from waste tire on the elemental mercury removal. Chem Eng J 2015;273:446–54.
- [22] Hsi HC, Chen CT. Influences of acidic/oxidizing gases on elemental mercury adsorption equilibrium and kinetics of sulfur-impregnated activated carbon. Fuel 2012;98:229–35.
- [23] Yao Y, Velpari V, Economy J. Design of sulfur treated activated carbon fibers for gas phase elemental mercury removal. Fuel 2014;116:560–5.
- [24] Li G, Shen B, Wang Y, Yue S, Xi Y, An M, et al. Comparative study of element mercury removal by three bio-chars from various solid wastes. Fuel 2015;145:189–95.
- [25] De M, Azargohar R, Dalai AK, Shewchuk SR. Mercury removal by bio-char based modified activated carbons. Fuel 2013;103:570–8.
- [26] Li G, Shen B, Li Y, Zhao B, Wang F, He C, et al. Removal of element mercury by medicine residue derived biochars in presence of various gas compositions. J Hazard Mater 2015;298:162–9.
- [27] Ahmad M, Rajapaksha AU, Lim JE, Zhang M, Bolan N, Mohan D, et al. Biochar as a sorbent for contaminant management in soil and water: a review. Chemosphere 2014;99:19–33.
- [28] Zhu C, Duan Y, Wu CY, Zhou Q, He M, Yao T, et al. Mercury removal and synergistic capture of SO₂/NO by ammonium halides modified rice husk char. Fuel 2016;172:160–9.
- [29] Yang W, Liu Z, Xu W, Liu Y. Removal of elemental mercury from flue gas using sargassum chars modified by NH₄Br reagent. Fuel 2018;214:196–206.
- [30] Tan Z, Niu G, Chen X. Removal of elemental mercury by modified bamboo carbon. Chin J Chem Eng 2015;23:1875–80.
- [31] Johari K, Saman N, Song ST, Chin CS, Kong H, Mat H. Adsorption enhancement of elemental mercury by various surface modified coconut husk as eco-friendly lowcost adsorbents. Int Biodeterior Biodegrad 2016;109:45–52.
- [32] Klasson KT, Boihem LL, Uchimiya M, Lima IM. Influence of biochar pyrolysis temperature and post-treatment on the uptake of mercury from flue gas. Fuel Process Technol 2014;123:27–33.
- [33] Shen B, Li G, Wang F, Wang Y, He C, Zhang M, et al. Elemental mercury removal by the modified bio-char from medicinal residues. Chem Eng J 2015;272:28–37.
- [34] Wang T, Liu J, Zhang Y, Zhang H, Chen WY, Norris P, et al. Use of a non-thermal plasma technique to increase the number of chlorine active sites on biochar for improved mercury removal. Chem Eng J 2018;331:536–44.
- [35] Chen WY, Mattern DL, Okinedo E, Senter JC, Mattei AA, Redwine CW. Photochemical and acoustic interactions of biochar with CO₂ and H₂O: applications in power generation and CO₂ capture. AIChE J 2014;60:1054–65.
- [36] Zhang Y, Zhang Z, Liu Z, Norris P, Pan WP. Study on the mercury captured by mechanochemical and bromide surface modification of coal fly ash. Fuel 2017;200:427–34.
- [37] Li G, Shen B, Li F, Tian L, Singh S, Wang F. Elemental mercury removal using biochar pyrolyzed from municipal solid waste. Fuel Process Technol 2015;133:43–50.
- [38] Wang J, Zhang Y, Han L, Chang L, Bao W. Simultaneous removal of hydrogen sulfide and mercury from simulated syngas by iron-based sorbents. Fuel 2013:103:73-9
- [39] Gu Y, Zhang Y, Lin L, Xu H, Orndorff W, Pan WP. Evaluation of elemental mercury adsorption by fly ash modified with ammonium bromide. J Therm Anal Calorim 2015;119:1663–72.
- [40] Wang F, Wang S, Meng Y, Zhang L, Wu Q, Hao J. Mechanisms and roles of fly ash compositions on the adsorption and oxidation of mercury in flue gas from coal combustion. Fuel 2016;163:232–9.
- [41] Zhou X, Huang X, Xie A, Luo S, Yao C, Li X, et al. V₂O₅-decorated Mn-Fe/attapulgite catalyst with high SO₂ tolerance for SCR of NO_x with NH₃ at low temperature. Chem Eng J 2017;326:1074–85.
- [42] Huang ZB, Liu BS, Tang XY, Wang XH, Amin R. Performance of rare earth oxide doped Mn-based sorbent on various silica supports for hot coal gas desulfurization. Fuel 2016;177:217–25.
- [43] Zhang J, Duan Y, Zhou Q, Zhu C, She M, Ding W. Adsorptive removal of gas-phase mercury by oxygen non-thermal plasma modified activated carbon. Chem Eng J 2016;294:281–9.
- [44] Zhang B, Xu P, Qiu Y, Yu Q, Ma J, Wu H, et al. Increasing oxygen functional groups of activated carbon with non-thermal plasma to enhance mercury removal efficiency for flue gases. Chem Eng J 2015;263:1–8.
- [45] Zhang B, Zeng X, Xu P, Chen J, Xu Y, Luo G, et al. Using the novel method of nonthermal plasma to add Cl active sites on activated carbon for removal of mercury from flue gas. Environ Sci Technol 2016;50:11837–43.
- [46] Wu S, Katayama R, Uddin MA, Sasaoka E, Xie ZM. Study on reactivity of HgO over activated carbon with HCl and SO₂ in the presence of moisture by temperatureprogrammed decomposition desorption mass spectrometry. Energy Fuels 2015;29:6598–604.
- [47] Wu S, Uddin MA, Nagano S, Ozaki M, Sasaoka E. Fundamental study on decomposition characteristics of mercury compounds over solid powder by temperature-programmed decomposition desorption mass spectrometry. Energy Fuels 2011;25:144–53.